Polymer Conductivity through Particle Connectivity

Joung Eun Yoo,[†,§] William P. Krekelberg,[§] Yangming Sun,[‡] Jacob D. Tarver,[†] Thomas M. Truskett,[§] and Yueh-Lin Loo*[,†]

Department of Chemical Engineering, Princeton University, Princeton, New Jersey 08544, and Departments of Chemical Engineering and Chemistry and Biochemistry, University of Texas at Austin, Austin, Texas 78712

Received February 11, 2009. Revised Manuscript Received March 10, 2009

Conducting polymers, especially those template-synthesized on polymer acids, have attracted considerable attention for applications in organic and polymer electronics because of their processability and patternability, excellent mechanical properties, and robust electronic properties. The template synthesis of conductive polymers with polymer acids in aqueous media results in electrostatically stabilized submicrometer particles. With a model system of polyaniline that is template-synthesized in a presence of poly(2-acrylamido-2-methyl-1-propanesulfonic acid), or PAAMPSA, we show that the molecular characteristics of PAAMPSA influence the size and size distribution of the particles. We further demonstrate that it is the packing of these particles that governs macroscopic conduction in the solid state. Accordingly, the macroscopic conductivity of such polymers scales linearly with particle density.

Introduction

Water-dispersible, polymer-acid-templated conductive polymers are widely used as hole injection layers in organic light-emitting diodes,[1,2] buffer layers,[3,4] and hole transport layers[5,6] within organic solar cells and as source and drain electrodes in organic thin-film transistors.[7−9] Despite their widespread use, the materials properties of such water-dispersible conductive polymer systems are highly variable depending on the details of synthesis and processing. Depending on the functional group of the polymer acid template, for example, the electrical conductivities of solution-processable poly(ethylene dioxythiophene), PEDOT, and polyaniline, PANI, derivatives can vary by several orders of magnitude. The conductivity of PANI can also vary dramatically depending on the molecular characteristics of the polymer acid.[10,11] Post-synthesis processing can also have profound effects on the electronic properties of PANI. The presence of moisture, for instance, can alter the work function of PEDOT by as much as 0.8 eV.[12,13] Post-deposition exposure of PEDOT to a "secondary dopant", such as ethylene glycol[14] or dimethylsulfoxide,[15] can dramatically increase its electrical conductivity; the origin of this conductivity enhancement, however, remains poorly understood. Given the promise of organic electronics and the wide incorporation of conductive polymers within these devices, it is imperative that we understand the factors that govern the electronic and electrical properties of these materials. With a model conductive polymer system of PANI that is template synthesized on poly(2-acrylamido-2-methyl-1-propanesulfonic acid), PAAMPSA, we demonstrate that the bulk conductivity of water-dispersible conductive polymers is dependent on a single parameter reducible from the molecular characteristics of the polymer acid. In particular, polymer-acid-template synthesis of conductive polymers results in electrostatically stabilized colloidal particles whose size and size distribution depend on the details of the synthetic parameters. When drop-cast as films, it is the number density of these particles that governs the macroscopic conduction of the conductive polymer.

Experimental Section

PAAMPSA was synthesized by conventional free-radical polymerization according to previously published procedures.[16,17] We also synthesized the polymer acid by atom transfer radical polymerization (ATRP)[18,19] to ensure that it had a narrower molecular

* To whom correspondence should be addressed. E-mail: lloo@princeton.edu.
† Princeton University.
§ Department of Chemical Engineering, University of Texas at Austin.
‡ Department of Chemistry and Biochemistry, University of Texas at Austin.

(1) Tessler, N.; Medvedev, V.; Kazes, M.; Kan, S.; Banin, U. *Science* **2002**, *295*, 1506.
(2) Friend, R. H.; Gymer, R. W.; Holmes, A. B.; Burroughes, J. H.; Marks, R. N.; Taliani, C.; Bradley, D. D. C.; Santos, D. A. D.; Bredas, J. L.; Logdlund, M.; Salaneck, W. R. *Nature (London)* **1999**, *397*, 121.
(3) Kim, J.; Khang, D.-Y.; Kim, J.-H.; Lee, H. H. *Appl. Phys. Lett.* **2008**, *92*, 133307.
(4) Li, G.; Chu, C.-W.; Shrotriya, V.; Huang, J.; Yang, Y. *Appl. Phys. Lett.* **2006**, *88*, 253503.
(5) Kim, J. Y.; Lee, K.; Coates, N. E.; Moses, D.; Nguyen, T.-Q.; Dante, M.; Heeger, A. J. *Science* **2007**, *317*, 222.
(6) Huynh, W. U.; Dittmer, J. J.; Alivisatos, A. P. *Science* **2002**, *295*, 2425.
(7) Lee, K. S.; Blanchet, G. B.; Gao, F.; Loo, Y.-L. *Appl. Phys. Lett.* **2005**, *86*, 074102.
(8) Lee, K. S.; Smith, T. J.; Dickey, K. C.; Yoo, J. E.; Stevenson, K. J.; Loo, Y.-L. *Adv. Func. Mater.* **2006**, *16*, 2409.
(9) Lee, C. S.; Kim, J. Y.; Lee, D. E.; Joo, J.; Wagh, B. G.; Han, S.; Beag, Y. W.; Koh, S. K. *Synth. Met.* **2003**, *139*, 457.
(10) Yoo, J. E.; Bucholz, T. L.; Jung, S.; Loo, Y.-L. *J. Mater. Chem.* **2008**, *18*, 3129.
(11) Yoo, J. E.; Cross, J. L.; Bucholz, T. L.; Lee, K. S.; Espe, M. P.; Loo, Y.-L. *J. Mater. Chem.* **2007**, *17*, 1268.
(12) Koch, N.; Vollmer, A.; Elschner, A. *Appl. Phys. Lett.* **2007**, *90*, 043512.
(13) Lee, T.-W.; Chung, Y. *Adv. Funct. Mater.* **2008**, *18*, 1.
(14) Ouyang, J.; Chu, C.-W.; Chen, F.-C.; Xu, Q.; Yang, Y. *Adv. Funct. Mater.* **2005**, *15*, 203.
(15) Kim, J. Y.; Jung, J. H.; Lee, D. E.; Joo, J. *Synth. Met.* **2002**, *126*, 311.

10.1021/cm900404e CCC: $40.75
Published on Web 04/07/2009

weight distribution compared to PAAMPSA. We separately refer to these materials as aPAAMPSA. Table S1 in the Supporting Information lists the relevant molecular characteristics of the polymer acids, including the poly(ethylene oxide) equivalent number-average molecular weight and the polydispersity index of PAAMPSA (and aPAAMPSA).

To synthesize PANI, PAAMPSA (or aPAAMPSA) is first dissolved in water. Aniline is then added and oxidatively polymerized along the polymer acid template. The detailed synthetic procedures have been outlined previously.[10,11] We refer to PANI that is template-synthesized on PAAMPSA as PANI−PAAMPSA and those template-synthesized on aPAAMPSA as PANI−aPAAMPSA. With increasingly more sulfonic acid groups involved in doping PANI during the course of polymerization, PAAMPSA becomes decreasingly hydrophilic; PANI−PAAMPSA forms submicrometer, electrostatically stabilized colloidal particles as a consequence. Given the strong ionic interactions between the sulfonic acid groups of PAAMPSA and the PANI backbone,[20] these particles are arrested during template synthesis; their characteristics do not change with further processing.

To characterize the size and size distribution of PANI−PAAMPSA (and PANI−aPAAMPSA) particles, we conducted dynamic light scattering (DLS) on dilute dispersions. Specifically, DLS experiments were conducted on 0.0001 wt % PANI−PAAMPSA (or PANI−aPAAMPSA) in 0.1 M NaCl aqueous solution at 25 °C. NaCl was added to screen interparticle electrostatic interactions. This salt concentration was selected after a series of control experiments carried out at varying salt and polymer concentrations (see Supporting Information for more details). As such, the mean hydrodynamic diameters extracted from these measurements reflect those of individual, isolated spherical particles.[21] A total of 7 runs of 10 scans each (at 10 s per scan) at 25 °C were conducted for all PANI−PAAMPSA (and PANI−aPAAMPSA) dispersions. The variations in the runs were used to determine the standard deviation on the mean hydrodynamic diameter and its distribution. We quantified the particle size distribution by characterizing the full width of the number-weighted intensity distribution at half the maximum intensity (FWHM). Measurements were carried out with a Brookhaven Instruments Inc. BI-200SM, equipped with a neodymium-doped yttrium aluminum garnet (Nd:YAG) laser that operates at 532 nm and an ALV 5000 autocorrelator at normal incidence. The correlation functions were analyzed using the CONTIN algorithm with inverse Laplace transformation. The size distributions reported herein are number-weighted intensity distributions from DLS. The mean hydrodynamic diameters as well as the FWHM of PANI−PAAMPSA (and PANI−aPAAMPSA) particles are tabulated in Table S1.

We also conducted transmission electron microscopy (TEM) to estimate the size of PANI−PAAMPSA (and PANI−aPAAMPSA) particles. For TEM experiments, dilute PANI−PAAMPSA (and PANI−aPAAMPSA) dispersions that were originally prepared for DLS experiments were drop-cast on copper grids. Excess water was wicked away with a piece of filter paper. A Zeiss 910 operating at 100 keV was used to acquire images.

The solid-state structures of PANI−PAAMPSA (and PANI−aPAAMPSA) were obtained on an atomic force microscope (AFM, Digital Instrument Nanoscope IIIa). Spin-coated PANI−PAAMPSA (and PANI−aPAAMPSA) films were prepared by spin-coating 5 wt % PANI−PAAMPSA (or PANI−aPAAMPSA) aqueous dispersions at 1000 rpm for 1 min on silicon wafers. The root-mean-square (rms) roughness of PANI−PAAMPSA (and PANI−aPAAMPSA) was quantified using NanoScope software ver.7.00b20.

The electrical conductivities were measured using the transmission-line method[22,23] and the four-probe method[7] at room temperature with an Agilent 4145B Semiconductor Parameter Analyzer. 5 wt % PANI−PAAMPSA dispersions were prepared in water and stirred for 10 days. The polymer dispersions were then drop-cast onto glass substrates with predefined gold electrodes. The films were left out to dry for 2 h before the electrical measurements. To extract electrical conductivities using the transmission-line method, the resistances between pairs of gold electrodes were measured and plotted against the distances between electrodes (100−300 μm); the conductivity of the specimen was extracted from the inverse slope of the data. During four-probe experiments, four gold electrodes that were equally spaced 4.0 mm apart were employed. The potential drop across the inner electrodes was normalized by the current measured across the two outer electrodes to yield a resistance that is free of parasitics. The inverse of this quantity gave us the conductivity of the sample. We have made multiple drop-cast films from different batches of dispersions and different batches of polymerizations for each sample; the conductivities of all of these films, whether extracted from the transmission-line experiments or the four-probe measurements, were averaged to yield the conductivity reported in Table S1. In each of these methods, we used the same stencil masks to define electrical contacts so the relative errors due to geometrical factors and dimension measurements are zero across all samples. The standard deviations reported in Table S1 thus reflect experimental errors in thickness measurements. The thickness of the films was measured using a Dektek II.

X-ray photoelectron spectroscopy was conducted using a Physical Electronics ESCA 5700 spectrophotometer equipped with a monochromatic Al Kα X-ray source and a hemispherical analyzer. All spectra were collected at a base pressure of 8×10^{-10} Torr and a sample current of 1.5 μA. Sputtering of PANI−PAAMPSA was performed with an Ar^+ gun at an ionization energy of 250 eV. The sputtering rate was estimated to be approximately 15 nm/min. High-resolution scans in the nitrogen and sulfur regions were acquired at 0.1 eV increments with a sweep time of 1000 ms/eV and 10 energy sweeps for each region. During data analysis, the XPS spectra were all shifted so the binding energy of C 1s occurred at 284.5 eV to compensate for any possible charging effects due to sputtering.[24,25] After baseline subtraction using a Shirley background,[26] the nitrogen and sulfur high-resolution spectra were deconvoluted with Gaussian functions using nonlinear least-squares analysis. During peak fitting in the nitrogen and sulfur regions, the full widths at half the maximum intensity (FWHM) of the peaks and the peak positions were kept constant, with peak intensities being the only floating parameters. Specifically, the nitrogen region was deconvoluted into three individual peaks at 399.2, 400.4, and 401.3 eV accordingly to published peak assignments.[27,28] The FWHM of the individual peaks were kept constant at 1.4 eV.[27,28] The XPS data in the sulfur region were deconvoluted into three

(16) Rosa, F.; Bordado, J.; Casquilho, M. *J. Appl. Polym. Sci.* **2003**, *87*, 192.
(17) Rivas, B. L.; Pooley, S. A.; Luna, M.; Geckeler, K. E. *J. Appl. Polym. Sci.* **2001**, *82*, 22.
(18) Bucholz, T. L.; Li, S. P.; Loo, Y.-L. *J. Mater. Chem.* **2008**, *18*, 530.
(19) Bucholz, T. L.; Loo, Y.-L. *Macromolecules* **2006**, *39*, 6075.
(20) Sun, L.; Yang, S. C.; Liu, J.-M. *Polym. Prepr.* **1992**, *33*, 379.
(21) Sedlak, M. *Langmuir* **1999**, *15*, 4045.
(22) Luan, S.; Neudeck, G. W. *J. Appl. Phys.* **1992**, *72*, 766.
(23) Zaumseil, J.; Baldwin, K. W.; Rogers, J. A. *J. Appl. Phys.* **2003**, *93*, 6117.
(24) Chan, H. S.; Munro, H. S.; Davies, C.; Kang, E. T. *Synth. Met.* **1988**, *22*, 365.
(25) Snauwaert, P.; Lazzaroni, R.; Riga, J.; Verbist, J. J. *Synth. Met.* **1987**, *16*, 245.
(26) Shirley, D. A. *Phys. Rev. B* **1972**, *5*, 4709.
(27) Kang, E. T.; Neoh, K. G.; Tan, K. L. *Prog. Polym. Sci.* **1998**, *23*, 277.
(28) Yue, J.; Epstein, A. J. *Macromolecules* **1991**, *24*, 4441.

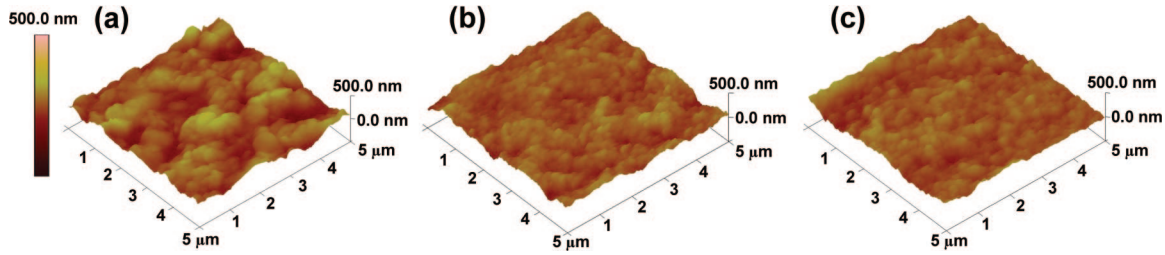

Figure 1. Atomic force microscopy topographical images of (a) PANI−PAAMPSA−724 (rms roughness of ≈60.3 nm), (b) PANI−PAAMPSA−45 (rms roughness of ∼41.5 nm), and (c) PANI−aPAAMPSA−30 (rms roughness of ≈36.4 nm).

doublets with individual peaks at the following: 163.5 and 164.7 eV; 167.5 and 168.7 eV; and 168.3 and 169.5 eV.[15,29,30] The individual peaks maintained a FWHM of 1.0 eV during peak fitting.[15,29,30] Given that the integrated peak intensity is proportional to the concentration of the individual species, the relative concentration of protonated nitrogens was determined by normalizing the integrated peak intensities associated with N_2^+ by the total nitrogen content. Similarly, the relative concentration of ionizied sulfonic acid was determined by normalizing its integrated peak intensity with that of total sulfur content. Changes in the relative concentrations with film depth were obtained by normalizing the relative concentrations against that obtained in the surface scan.

During simulations, we accounted for the packing of the particles in the film by considering the particles to have the experimentally determined size distribution, scaled in each system to yield approximately 2000 particles, and assuming hard sphere interparticle interactions. We simulated the "concentration" of this hard-sphere system using the Lubachevsky-Stillinger algorithm.[31] In this method, event-driven molecular dynamics for the particles was carried out in a periodically replicated simulation cell.[32] Specifically, the simulation cell volume was kept constant, and the radius of each particle was allowed to "grow" linearly in time until the system reached a jammed state.[33−35] As shown in the Supporting Information, our simulations provided evidence that one can accurately estimate the final particle surface area per film volume for each experiment, A_i/V (or alternatively, the number density of particles, ρ_i), given the experimental particle-size distribution and by assuming that all systems have the same packing fraction, ϕ_i.

Results and Discussion

We chose PAAMPSA as our polymer acid template because its amide groups can hydrogen bond with water so PAAMPSA is more "hydrophilic" compared to the more conventional polymer acid template of poly(styrene sulfonic acid).[7] More importantly, its sulfonic acid groups can proton-dope PANI to render electrical conductivity while excess sulfonic acid groups promote water dispersibility, thereby solution processability. To examine how the molecular parameters of PAAMPSA influence the macroscopic electrical properties of PANI−PAAMPSA, we synthesized two series of polymer acid templates as a function of molecular weight, one by conventional free-radical polymerization so the molecular weight distribution of PAAMPSA is broad (characterized by polydispersity index (PDI) ≥ 1.4) and the other series by ATRP so the molecular weight distribution of the polymer acid is narrow in comparison (PDI ≤ 1.3).[10,11] Figure 1 shows AFM micrographs of several films of PANI−PAAMPSA of varying polymer acid molecular weight and molecular weight distribution drop cast from 5 wt % aqueous dispersions. The micrograph of PANI−PAAMPSA−724, which was template polymerized on PAAMPSA having a molecular weight of 724 kg/mol and a PDI of 1.64, is highly irregular and reveals large particles of approximately a micrometer in size (Figure 1a). The rms roughness of this film is 60.3 nm. Given the polydispersity in the size of the particles, it is not surprising that the roughness is only a fraction of the mean particle size.[36] Similarly drop-cast PANI−PAAMPSA−724 films exhibit a conductivity of 0.43 ± 0.02 S/cm. In contrast, the micrograph of PANI−PAAMPSA−45, which was template synthesized on PAAMPSA having a molecular weight of 45 kg/mol and a PDI of 1.43, appears smoother (Figure 1b); smaller particles make up this film having a rms roughness of 41.5 nm. The conductivity of PANI−PAAMPSA−45 films is 1.09 ± 0.03 S/cm. The micrograph of PANI−aPAAMPSA−30 is shown in Figure 1c. This PANI was derived from the template polymerization of aniline on aPAAMPSA having a molecular weight of 30 kg/mol, but a significantly reduced PDI of 1.16. The particles in PANI−aPAAMPSA−30 appear to be comparable in size with those in PANI−PAAMPSA−45 and the film is characterized by a rms roughness of 36.4 nm. PANI−aPAAMPSA−30 films exhibit a conductivity of 2.39 ± 0.03 S/cm. Figure 2 plots the electrical conductivity of PANI−PAAMPSA (and PANI−aPAAMPSA) as a function of the molecular weight of the polymer acid for all the samples examined. With decreasing polymer acid molecular weight, the electrical conductivity of PANI−PAAMPSA (and PANI−aPAAMPSA) increases. The electrical conductivity further increases by a factor of 2 to 3 when a polymer acid of comparable molecular weight but narrower molecular weight distribution is used to template synthesize PANI. Strong correlations thus exist between the molecular characteristics of the polymer acid

(29) Greczynski, G.; Kugler, T.; Salaneck, W. R. *Thin Solid Films* **1999**, *354*, 129.
(30) Xing, K. Z.; Fahlman, M.; Chen, X. W.; Inganaes, O.; Salaneck, W. R. *Synth. Met.* **1997**, *89*, 161.
(31) Lubachevsky, B. D.; Stillinger, F. H. *J. Stat. Phys.* **1990**, *60*, 561.
(32) Rapaport, D. C. *The Art of Molecular Dynamics Simulation*, 2nd ed.; Cambridge University Press: Cambridge, 2004.
(33) Torquato, S.; Truskett, T. M.; Debenedetti, P. G. *Phys. Rev. Lett.* **2000**, *84*, 2064.
(34) Song, C.; Wang, P.; Makse, H. A. *Nature (London)* **2008**, *453*, 629.
(35) Truskett, T. M.; Torquato, S.; Debenedetti, P. G. *Phys. Rev. E* **2000**, *62*, 993.
(36) Reyes, Y.; Campos-Teran, J.; Vazquez, F.; Duda, Y. *Modelling Simul. Mater. Sci. Eng.* **2007**, *15*, 355.

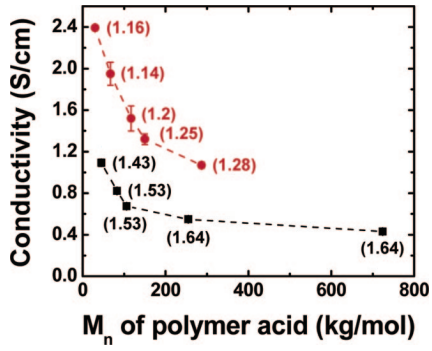

Figure 2. Bulk conductivities of PANI−PAAMPSA (■) and PANI−aPAAMPSA (●) with varying PAAMPSA (and aPAAMPSA) molecular weights. The PDIs of PAAMPSA (and aPAAMPSA) are labeled in brackets accordingly.

and the electrical conductivity of the resulting PANI−PAAMPSA (and PANI−aPAAMPSA).[10,11]

Given the differences in the solid-state structures of PANI−PAAMPSA (and PANI−aPAAMPSA), we surmise that how these electrostatically stabilized colloidal particles pack when drop cast as films must influence macroscopic conduction in these materials. To assess how PANI−PAAMPSA (and PANI−aPAAMPSA) particles pack, we need to first obtain quantitative information about the size and size distribution of the particles that are involved. We thus turned to DLS experiments on dilute aqueous dispersions of 0.0001 wt % PANI−PAAMPSA (and PANI−aPAAMPSA) in 0.1 M NaCl to quantify the mean particle size and size distribution. Figure 3 contains the number-weighted size distribution of PANI−PAAMPSA−724, PANI−PAAMPSA−45, and PANI−aPAAMPSA−30 from such DLS experiments. The mean hydrodynamic diameters extracted from these distributions are 1230 ± 25, 543 ± 9, and 560 ± 11 nm, respectively, for the three PANI−PAAMPSA (and PANI−aPAAMPSA) complexes. To confirm that the mean hydrodynamic diameters truly represent the size of isolated individual particles and not aggregates due to interparticle electrostatic interactions,[21] we carried out transmission electron microscopy (TEM) on PANI−PAAMPSA and PANI−aPAAMPSA. TEM specimens were prepared by drop-casting the same dilute aqueous dispersions used in DLS experiments on copper grids. Representative TEM micrographs of PANI−PAAMPSA−724, PANI−PAAMPSA−45, and PANI−aPAAMPSA−30 are shown in Figures 3d−f. These particles appear to be spherical and their sizes consistent with those extracted from DLS. We did not see any evidence of aggregation during TEM experiments. Collectively, our experiments indicate that PANI−PAAMPSA (and PANI−aPAAMPSA) particle size increases with increasing molecular weight of PAAMPSA. We also characterized the size distribution of the particles by quantifying the FWHM of the DLS intensity distribution. The FWHM of the intensity distributions of PANI−PAAMPSA−724, PANI−PAAMPSA−45, and PANI−aPAAMPSA−30 are 926 ± 69, 636 ± 12, and 374 ± 4 nm, respectively. The size distribution of the particles thus scales with the molecular weight distribution of the polymer acid. Accordingly, the relationship between the molecular characteristics of PAAMPSA (or aPAAMPSA) and the size and size distribution of PANI−PAAMPSA (or PANI−aPAAMPSA) particles implicates a correlation between the characteristics of the particles and the macroscopic electrical properties of PANI−PAAMPSA (and PANI−aPAAMPSA), with smaller particles and those of narrower size distribution leading to higher conductivities when PANI−PAAMPSA (or PANI−aPAAMPSA) is cast as films.

To address how the particles pack when cast as films, we quantified the connectivity of the particles given our DLS results based on eq 1 below:

$$\varphi_i = \frac{4\pi}{3}\rho_i \int_0^\infty r^3 f_i(r)\, dr \qquad (1)$$

In eq 1, $f_i(r)$ is the normalized particle size distribution that is experimentally obtained by DLS of specimen i and ρ_i is the number density of particles. Given that PANI−PAAMPSA (and PANI−aPAAMPSA) particles are spherical and individually isolated, we assumed that our materials system can be adequately modeled with hard-sphere interparticle interactions. Assuming hard spheres with radius r, the macroscopic packing fraction, ϕ_i, can be estimated. Alternatively, if ϕ_i is known, one can estimate the number density of particles within a solid film, given the intensity distributions from DLS. We have performed extensive molecular dynamics simulations of film formation of PANI−PAAMPSA (see details in the Supporting Information). Provided that crystallization is avoided, these simulations demonstrate that the macroscopic packing fraction, ϕ_i, is largely independent of particle size and size distribution and is insensitive to the rate at which the particles are concentrated during film formation. Of simulations carried out with the intensity distributions from DLS using the fastest concentration rate, $\phi_i = 0.649 \pm 0.007$. Given the DLS intensity distributions and assuming a constant ϕ_i across all samples (see Supporting Information for numerical justification), we are thus able to estimate ρ_i for individual PANI−PAAMPSA and PANI−aPAAMPSA specimens.

Figure 4a plots the conductivity of PANI−PAAMPSA (and PANI−aPAAMPSA) as a function of ρ_i. A total of 12 PANI−PAAMPSA (and PANI−aPAAMPSA) specimens synthesized on polymer acid templates having varying molecular characteristics were examined. We observe that the conductivity of PANI−PAAMPSA (and PANI−aPAAMPSA) scales linearly with a single parameter, i.e., ρ_i, reducible from the molecular characteristics of PAAMPSA (and aPAAMPSA). To further explore how the conductivity is influenced by the connectivity of these particles in the solid state, we estimated the particle surface area per unit volume of the cast film, A_i/V, based on eq 2 below:

$$A_i/V = 4\pi\rho_i \int_0^\infty r^2 f_i(r)\, dr \qquad (2)$$

The variation of electrical conductivity of PANI−PAAMPSA (and PANI−aPAAMPSA) with A_i/V is plotted in Figure 4b. We observe that the conductivity increases superlinearly with A_i/V, suggesting that charge transport does not occur through the bulk of the particles. If macroscopic conduction were to occur through the bulk of the particles (i.e., if the particles were chemically homogeneous), one would expect the conductivity to be—at best—constant with

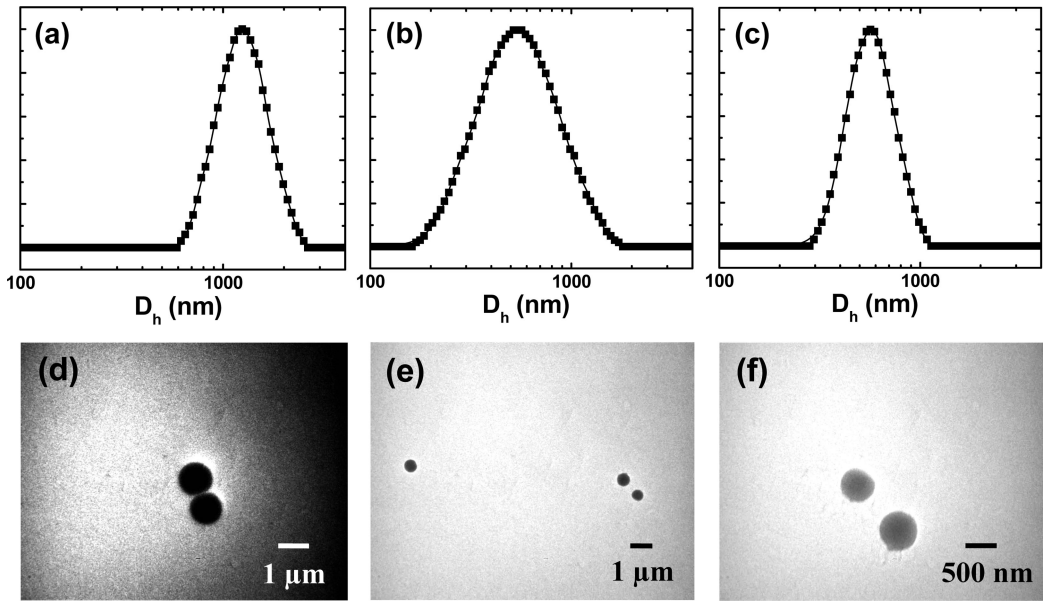

Figure 3. Particle size distributions of (a) PANI−PAAMPSA−724, (b) PANI−PAAMPSA−45, and (c) PANI−aPAAMPSA−30 measured by dynamic light scattering at 25 °C in 0.1 M NaCl (0.0001 wt % polymer); transmission electron microscopy images of (d) PANI−PAAMPSA−724, (e) PANI−PAAMPSA−45, and (f) PANI−aPAAMPSA−30 revealing individual spherical particles whose sizes are consistent with those measured by DLS.

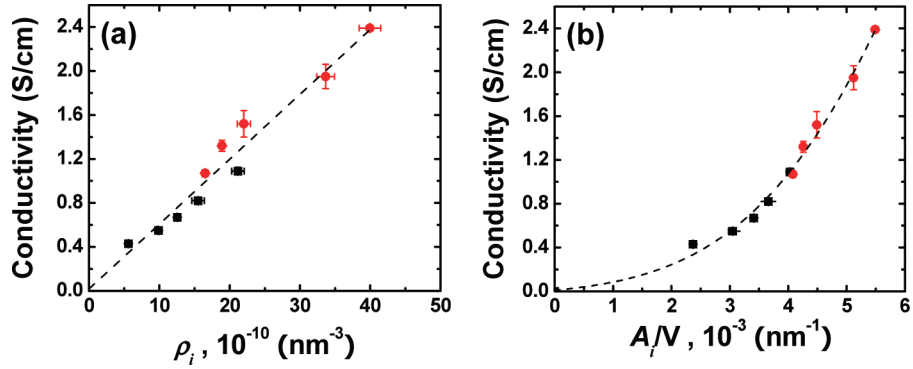

Figure 4. Conductivities of PANI−PAAMPSA (■) and PANI−aPAAMPSA (●) as a function of (a) particle number density, ρ_i, and (b) particle surface area per unit cast film, A_i/V, respectively. ρ_i and A_i/V are calculated based on the assumption of $\phi_i = 0.64$ for all polymers examined. A fit (dashed line) to the data is included in each graphic.

increasing A_i/V since the macroscopic volume fractions for all the samples are comparable. In fact, and perhaps more realistically, particle−particle contacts along the conduction paths provide points of resistance, and since their numbers generally increase with A_i/V, one would expect the conductivity to decrease with A_i/V for films comprising chemically homogeneous particles. Because conductivity increases with A_i/V in PANI−PAAMPSA (and PANI−aPAAMPSA), we are left to hypothesize that the conductive portions are preferentially segregated to the surface of the particles.

The notion of surface-mediated conduction is surprising in polymer-acid-templated conductive polymer systems and necessitates that the PANI−PAAMPSA (and PANI−aPAAMPSA) particles are compositionally heterogeneous. Specifically, the surface of the particles must be more conductive than the interior for conduction to preferentially occur along the surface. This observation is in contrast with what is known for commercially available PEDOT−PSS, where a thin overlayer of the insulating polymer acid is frequently observed.[37,38] This PSS overlayer not only hinders macroscopic conduction but also can change the work function of PEDOT−PSS depending on the exposed humidity.[12] We carried out depth profile measurements in conjunction with X-ray photoelectron spectroscopy (XPS) to examine the concentration profile of PANI−PAAMPSA−724. An argon ion beam was used to sputter-etch PANI−PAAMPSA−724 for 5−10 min intervals and XPS measurements were conducted after each interval to probe the changes in the chemical environment with film depth.

Parts (a) and (b) of Figure 5 contain high-resolution XPS spectra in the nitrogen and sulfur regions, respectively, with increasing film depth. The nitrogen spectrum was deconvoluted into three components: a peak located at 399.2 eV attributed to the amide groups in PAAMPSA; one centered at 400.4 eV attributed to the protonated nitrogens associated with polarons and bipolarons in PANI−PAAMPSA (denoted N_1^+); and a third located at 401.3 eV attributed to protonated nitrogens that are ionically associated with the

(37) Hwang, J.; Amy, F.; Kahn, A. *Org. Electron.* **2006**, *7*, 387.
(38) Xing, K. Z.; Fahlman, M.; Chen, X. W.; Inganas, O.; Salaneck, W. R. *Synth. Met.* **1997**, *89*, 161.

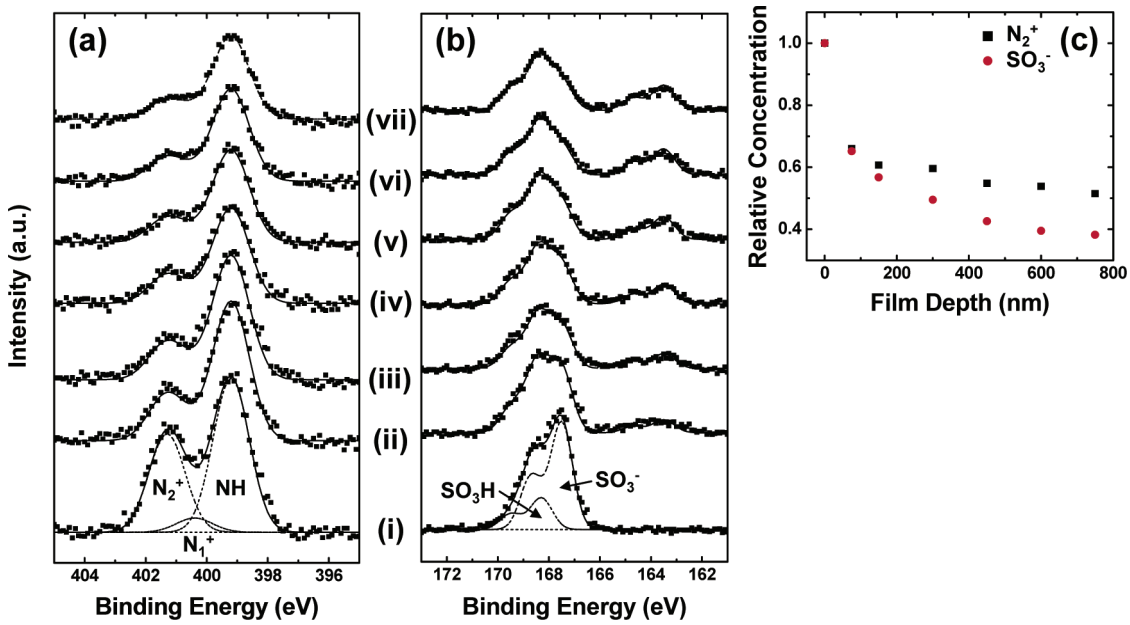

Figure 5. XPS spectra of the (a) nitrogen and (b) sulfur regions for (i) as-cast PANI−PAAMPSA−724 (with peak deconvolution) and the same film upon sputtering for (ii) 75 nm, (iii) 150 nm, (iv) 300 nm, (v) 450 nm, (vi) 600 nm, and (vii) 750 nm. The overall fit is shown with a solid line in each spectrum. The relative concentrations of protonated nitrogen (N_2^+, ■) and ionized sulfur ($-SO_3^-$, ●), normalized by the surface concentrations of the respective elements before sputtering, are shown in (c).

sulfonic acid groups in PAAMPSA (denoted N_2^+).[27,28] The concentration of protonated nitrogens is high in the surface scan (Figure 5a−i); its concentration decreases relative to that of the amide as we sputter into the PANI−PAAMPSA film. This trend is quantified in Figure 5c where the relative concentration of N_2^+, normalized to that on the surface, is plotted as a function of film depth. The concentration of N_2^+ decreases rapidly with film depth; it then levels off at approximately 300 nm below the surface. A similar analysis was carried out with the sulfur region of the XPS scans. The sulfur XPS scans can be deconvoluted into two sets of doublets: a pair with peaks located at 167.5 and 168.7 eV and another with peaks located at 168.3 and 169.5 eV.[15,30] The doublet at lower binding energy corresponds to sulfurs in the ionized sulfonic acid groups of PAAMPSA ($-SO_3^-$) while that at higher binding energy corresponds to sulfurs in the sulfonic acid groups of PAAMPSA ($-SO_3H$) that do not participate in the protonation of PANI.[15,30] With increasing film depth, the concentration of ionized sulfonic acid decreases relative to that of the neutral sulfonic acid. This trend is also quantified in Figure 5c where the relative concentration of ionized sulfonic acid, normalized by the surface concentration, is plotted with film depth. Similar to the concentration of protonated nitrogens, that of ionized sulfonic acid decreases rapidly with film depth; this decay slows down as we probe deeper into the film. We note, however, one subtlety between the decay in the relative concentration of N_2^+ and that of ionized sulfur. The relative concentration of N_2^+ plateaus at 300 nm below the film surface whereas the relative concentration of ionized sulfonic acid continues to decrease. We believe this difference is due to slight deterioration of the film by ion sputtering. Indeed, a careful inspection of the sulfur XPS spectra in Figure 5b reveals the emergence of an additional doublet whose peaks are at 163.5 and 164.7 eV; this doublet is attributed to elemental sulfur or thiol moieties ($-SH$).[39] The constant bombardment of argon ions can lead to oxygen loss within the sulfonic acid groups of PAAMPSA, which in turn leaves behind elemental sulfur or thiols. Such ion beam damage was previously reported during sputtering and depth profile experiments conducted on PEDOT−PSS.[39] Despite the slight film damage observed, however, our XPS depth profiling experiments convincingly indicate that the concentrations of the ionized species of PANI (protonated nitrogens) and PAAMPSA (ionized sulfonic acid groups) are preferentially enhanced on the exterior of the particles. We thus ascribe surface-mediated conduction in PANI−PAAMPSA (and PANI−aPAAMPSA) to the preferential enhancement of protonated nitrogen and ionized sulfonic acid groups at the surface of the particles.

Conclusions

The electrical properties of PANI−PAAMPSA (and PANI−aPAAMPSA)—like those of other polymer-acid-templated conductive polymers—depend strongly on the details of the synthesis parameters. But variations in the molecular characteristics of the polymer acid template can be reduced to a single parameter, to which the electrical conductivity in the solid state can be related. This finding is general and should be applicable to any conductive polymers that are derived from such a polymer acid template synthesis procedure. Such syntheses result in the formation of electrostatically stabilized colloidal particles, whose packing in the solid state dictates macroscopic conduction. The ability to relate variables that are tunable at the onset of synthesis to influence the characteristics of the particles presents new

(39) Crispin, X.; Marciniak, S.; Osikowicz, W.; Zotti, G.; Gon, A. W. D. V. D.; Louwet, F.; Fahlman, M.; Groenendaal, L.; Schryver, F. D.; Salaneck, W. R. *J. Polym. Sci., Part B: Polym. Phys.* **2003**, *41*, 2561.

opportunities to predict the electrical properties of conductive polymers a priori and, accordingly, to controllably manipulate design parameters for target properties.

Acknowledgment. The Keck Foundation, the Beckman Foundation through its Young Investigator Program, the National Science Foundation through CAREER awards to Y.-L.L. and T.M.T. (DMR-0753148 and CTS-028772), the Welch Foundation (F-1696), and the David and Lucile Packard Foundation have supported this work. We thank Andrey Dobrinin at the University of Connecticut and Antoine Kahn at Princeton University for useful discussions.

Supporting Information Available: This material is available free of charge via the Internet at http://pubs.acs.org.

CM900404E